

Neural Networks for Parameter Estimation in Intractable Models

Amanda Lenzi¹, Julie Bessac¹, Johann Rudi¹ and Michael L. Stein²

August 2, 2021

Abstract

We propose to use deep learning to estimate parameters in statistical models when standard likelihood estimation methods are computationally infeasible. We show how to estimate parameters from max-stable processes, where inference is exceptionally challenging even with small datasets but simulation is straightforward. We use data from model simulations as input and train deep neural networks to learn statistical parameters. Our neural-network-based method provides a competitive alternative to current approaches, as demonstrated by considerable accuracy and computational time improvements. It serves as a proof of concept for deep learning in statistical parameter estimation and can be extended to other estimation problems.

Keywords: Deep neural networks, intractable likelihood, max-stable distributions, parameter estimation

Short title: Deep learning for parameter estimation

¹Mathematics and Computer Science Division, Argonne National Laboratory, Lemont, IL, USA.

²Department of Statistics, Rutgers University, Piscataway, NJ, USA.

1 Introduction

The large datasets that are increasingly available because of advances in data storage and sensor technology inevitably display complex dependencies, bringing new opportunities and new challenges to statistical modeling and prediction. Environmental processes give an important example for which datasets can have complicated interactions across multiple scales of spatial and temporal variability. Specifically, inference for parametric statistical models designed for non-Gaussian data that account for spatiotemporal dependencies are computationally challenging. For instance, consider models for multivariate extremes, where data are usually sampled at a large number of spatial locations but large computational complexities limit their usefulness. In order to circumvent this bottleneck, model approximations that avoid full likelihood computation have been developed. One such approximation is based on composite likelihood, usually constructed from pairs of observations (Tawn, 1988; Padoan et al., 2010; Ribatet et al., 2012). However, even though the maximum pairwise likelihood estimator is strongly consistent and asymptotically normal under mild regularity conditions (Xu and Reid, 2011), no obvious strategy exists for selecting the composite likelihood terms optimally, and the loss in efficiency makes inference for high-dimensional data still challenging (Varin et al., 2011; Huser et al., 2016).

As an alternative to composite likelihood inference in models for spatial extremes, Stephenson and Tawn (2005) suggested augmenting the componentwise block maxima data with their occurrence times and showed that partitioning the locations based on whether maxima coincided simplifies the likelihood function substantially. To avoid the bias that emerges from fixing these partitions, Huser et al. (2019) constructed a stochastic expectation-maximization algorithm for exact maximum likelihood estimation of max-stable processes by treating the partitions as latent variables. Similarly, in a Bayesian setting, Thibaud et al. (2016) developed a Markov chain Monte Carlo algorithm for max-stable processes conditioning on the partition values. A possible problem with these approaches is that they assume independence in time, and how much bias this temporal dependence might cause is unclear. Moreover, likelihood-based techniques are still

hindered by the computational bottleneck of evaluating multivariate max-stable cumulative distribution functions. A key aspect of models for dependence is that often simulation is fast and tractable, although likelihood computation is burdensome. Taking advantage of that, Erhardt and Smith (2012) employed a simulation-based approach using approximate Bayesian computation (ABC) for estimating parameters of max-stable models. In its most basic form, ABC first samples a set of parameters from the prior distribution, which are then used to simulate data under the assumed statistical model. For each new dataset, a procedure of evaluating discrepancies between the simulations and the observed data must be repeated. As a result, neither of the previously mentioned approaches are well suited for large datasets. Therefore, developing new inference methods for computationally challenging likelihoods remains an open challenge, as is the case of max-stable processes and many other applications.

In this work we propose an approach to estimate the parameters of intractable statistical models using deep neural networks (NNs). Deep learning algorithms utilize NNs as multiple interconnected layers to predict or classify complex maps between datasets, and in recent years they have shown remarkable success at predicting high-dimensional nonlinear processes. Literature on deep NN techniques applied directly in the context of parameter estimation is scarce. Within the ABC framework, Creel (2017) proposed to use informative statistics to train a deep NN upon which classical or Bayesian indirect inference may be based. Jiang et al. (2017) predicted summary statistics from simulated data, which were then used as an estimate of the posterior mean of an ABC procedure. Recently, Radev et al. (2020) proposed to perform Bayesian inference using informative summary statistics from the data as the input to invertible NNs. However, these papers provide no general guidance on how to construct suitable summary statistics for the networks in practice. Convolutional neural networks (CNNs) have been successfully applied to represent covariance structures of Gaussian processes by using sensor measurements (Liu et al., 2018), time-series data (Cremanns and Roos, 2017), and spatial data (Gerber and Nychka, 2020). Rudi et al. (2021) proposed to solve a deterministic inverse problem using dense and

convolutional layers in NNs, where parameters from a nonlinear system of ordinary differential equations are estimated from simulated data. To our knowledge, the present work is the first study in which deep NN methodologies are utilized with the goal of performing inference based solely on simulated data and parameters.

Similar to ABC, we perform statistical inference based on simulations rather than direct evaluations of computationally expensive or intractable likelihood functions. A crucial difference from ABC is that instead of measuring similarity as a function of informative summary statistics of the simulated data with the actual observations, our approach learns to perform the mapping directly between data and parameters. Therefore, our method can be seen as a form of automatic ABC, where the data compression is done inside the NN without the difficulties of picking potentially highly sensitive metrics. Our new construction uses simulated data from the statistical model as the input to a deep NN. The output consists of the parameters used to simulate the input data. We leverage the feasibility to simulate arbitrarily large amounts of training data in order to ensure that the deep NNs approximate the actual parameters as well as possible. After the deep NN is trained, the observed data are used as the input in the testing data, returning the model parameters of interest as output. We show that the deep NN can estimate parameters of max-stable models for spatial extremes with higher accuracy than traditional (approximate) likelihood approaches can, with a considerable speed-up in computations. As the number of parameters increases, a substantial decrease in the computational efficiency is observed for ABC methods, and the same will likely occur with our proposed framework. This work holds promising results for parameter estimation and serves as a proof of concept on how machine learning can be used for statistical inference when the traditional techniques fail.

We demonstrate our framework on a problem of determining parameters from max-stable models. Spatial data in extremes can be viewed as a particular case of 2D images, making NNs with convolutional layers a promising candidate due to their success in learning features of complex images. In this work we initially carry out simulated examples for Brown—Resnick

(Kabluchko et al., 2009) and Schalthers’s (Schlather, 2002) models and compare the accuracy of our approach with the standard pairwise likelihood technique. We show that CNN architectures are fast to fit and can provide less biased and less variable predictions than the typical approaches provide. Then, using 10-day blocks of reanalysis temperature data in the midwestern United States, we illustrate the performance and benefits of the proposed framework in terms of accuracy and computational savings over the standard approach. Another advantage of our approach over pairwise likelihood estimation methods is that no detailed knowledge in the field (e.g., extremes) is necessary since the target statistical computation is done inside the deep NN. Therefore, our deep NN-based framework does not require any assumptions about the data generation process. Instead, it is designed to have a flexible and computationally appealing form, with the network’s weights learned by training, which allows accurate representation of a large class of functions. Although our focus is on spatial extreme modeling, the new approach can be used for other inference problems as long as simulations from the probability model are possible.

The remainder of this paper is organized as follows. Section 2 provides an overview of the proposed approach and briefly introduces CNNs. In Section 3 we recall the definition of max-stable processes and inference based on pairwise likelihoods and conduct a simulation study to assess the performance of the estimators. In Section 4 we illustrate our method on a dataset of temperature minima, and we conclude with a discussion in Section 5.

2 Methodology

This section outlines our new framework for estimating parameters in statistical models by using deep NNs and gives a brief overview of the type of networks used in our examples.

2.1 Parameter estimation framework

In what follows, we will use the terminology *parameters* to refer to the parameters in statistical models of interest; the term *NN weights* denotes the parameters of NNs. As in classical statistical

inference, our goal is to use observed data to infer the underlying characteristics of a stochastic process by estimating parameters of an assumed probability model. Suppose Y is a random variable with values in a measurable space and probability density function p with respect to a reference measure μ (often the Lebesgue measure). Consider that the probability density function $p(\cdot; \boldsymbol{\theta})$ depends on a finite-dimensional parameter set $\boldsymbol{\theta} \in \Theta \subset \mathbb{R}^K$, where Θ denotes all possible values of $\boldsymbol{\theta}$ and $K \in \mathbb{N}$. The statistical problem is to recover the unknown $\boldsymbol{\theta}$ given $\mathbf{y} = (y_1, \dots, y_n)^\top$, where y_i are independent copies from $p(\cdot; \boldsymbol{\theta})$. Evaluating $p(\cdot; \boldsymbol{\theta})$ at observed data samples \mathbf{y} gives a real-valued function $p(\mathbf{y}; \boldsymbol{\theta})$, which is called the likelihood function. In most cases, this likelihood function is explicitly known and can be evaluated either analytically or numerically for pairs $(\mathbf{y}; \boldsymbol{\theta})$. To estimate $\boldsymbol{\theta}$, one commonly uses the principle of maximum likelihood, which assumes that the most reasonable values are those for which the density of the observed sample is largest. The value $\hat{\boldsymbol{\theta}} = \hat{\boldsymbol{\theta}}(\mathbf{y})$ that maximizes the log-likelihood function is called the maximum likelihood estimate (MLE):

$$\hat{\boldsymbol{\theta}} = \arg \max_{\boldsymbol{\theta} \in \Theta} p(\mathbf{y}; \boldsymbol{\theta}). \quad (1)$$

Often, however, no closed-form solution to the maximization problem is known or available, and the MLE can be found only via numerical optimization. In even more extreme cases, such as many non-Gaussian models for dependencies, writing down the full likelihood is impossible, and advanced numerical optimization strategies are impractical even at moderate dimensions.

We propose to tackle this problem using deep NNs, a type of machine learning that exploits a connected multilayer set of models to learn complex input-output maps. The idea is to use samples of parameters and data pairs to learn the function $p(\cdot; \boldsymbol{\theta})$. In other words, our goal is to find a useful approximation to $p(\cdot; \boldsymbol{\theta})$ that underlies the predictive relationship between $\boldsymbol{\theta}$ and \mathbf{y} . Our estimation technique is a deep NN taking \mathbf{y} as the independent input data and $\boldsymbol{\theta}$ as the dependent output data

$$\mathcal{F} : \mathbf{y} \mapsto \boldsymbol{\theta}; \quad \hat{\boldsymbol{\theta}} = \arg \min d\{\mathbf{y}, \mathcal{F}_{\mathbf{w}}(\boldsymbol{\theta})\}, \quad (2)$$

where $\mathcal{F}_{\mathbf{w}}$ is a function that depends on a set of l_1 deep NN weights and l_2 NN biases, in other words, $\mathbf{w} = (w_1, \dots, w_{l_1}, b_1, \dots, b_{l_2})^\top$. These weights are determined by training, whereas d in (2) represents a measure of distance between \mathbf{y} and $\mathcal{F}_{\mathbf{w}}(\boldsymbol{\theta})$. The function $\mathcal{F}_{\mathbf{w}}$ is analogous to the arg max operation, but it approximates the relation between \mathbf{y} and $\boldsymbol{\theta}$ by means of a deep NN instead of maximizing the likelihood function. In our approach we seek the function \mathcal{F} for predicting $\boldsymbol{\theta}$ given values of the input \mathbf{y} . This problem requires a criterion for choosing \mathcal{F} , namely, a loss function that penalizes errors in prediction. For regression problems, the mean squared error (MSE) loss is the most common and convenient choice (Friedman et al., 2001) and is given by

$$\text{MSE}(\mathbf{w}) = \mathbb{E}\{\boldsymbol{\theta} - \mathcal{F}_{\mathbf{w}}(\boldsymbol{\theta})\}^2. \quad (3)$$

An optimization algorithm uses the gradients, usually calculated via automatic differentiation (Paszke et al., 2017), of the loss function in (3) applied to the output of the deep NN and data. The idea is that the deep NN finds the set of weights \mathbf{w} such that the fit gets as close to the observed points as possible based on realizations of the output, where proximity is measured by the $\text{MSE}(\mathbf{w})$. For a linear model, a simple closed-form solution to the minimization problem of (3) exists; otherwise, the solution often requires iterative methods. Several numerical optimizers built around batch gradient descent methods are implemented to perform this task (e.g., see Kingma and Ba (2014)).

The problem of optimizing $\mathcal{F}_{\mathbf{w}}$ involves generating training data for the deep NN. For this purpose we produce training samples of parameters and data pairs $(\boldsymbol{\theta}_j^{\text{train}}, \mathbf{y}_j^{\text{train}})_{j=1}^J$, with $\boldsymbol{\theta}_j^{\text{train}} = (\theta_{1,j}, \dots, \theta_{K,j})^\top$ and $\mathbf{Y}_j^{\text{train}} = (y_{1,j}, \dots, y_{n,j})^\top$, where it is crucial that $\boldsymbol{\theta}_j^{\text{train}}$ corresponds to configurations covering the parameter domain of interest Θ . Different approaches can be used to find such configurations. One possible method is to obtain crude estimates of $\boldsymbol{\theta}$ from the observed data \mathbf{y} (e.g., using approximate maximum likelihood methods) and simulate $(\boldsymbol{\theta}_j^{\text{train}})_{j=1}^J$ in a large enough neighborhood of those. Then, after the parameter space Θ has been defined and samples of $(\boldsymbol{\theta}_j^{\text{train}})_{j=1}^J$ have been generated, these can be used to simulate corresponding data

samples $(\mathbf{y}_j^{\text{train}})_{j=1}^J$. The number of training samples depends on the difficulty of the problem and directly affects the quality of the estimator (Juba and Le, 2019). However, we find that appropriate transformations of the input and output greatly reduce the number of samples needed for decent accuracy. Once the deep NN has been trained, it can be used to accomplish our goal of performing statistical inference, namely, returning the probability model’s parameters based on new observed data.

2.2 Introduction to convolutional neural networks

Here we give details on the specific form assumed for $\mathcal{F}_{\mathbf{w}}$ in (2) responsible for learning the mapping between simulated data (input) and the statistical model parameters (output) of the deep NN. The choice of the deep neural network will likely depend on the type of input and output. In the following sections we analyze spatial 2D data; therefore, we focus on CNNs, a class of deep NNs most commonly applied to visual imagery that accounts for local dependencies in signals. We consider $\mathcal{F}_{\mathbf{w}}$ to be a composition of m nonlinear functions such that $\mathcal{F}_{\mathbf{w}}(\boldsymbol{\theta}) = (f_m \circ f_{m-1} \circ \dots \circ f_1)(\boldsymbol{\theta})$, where each $f(\cdot)$ is a function of at least one hidden layer. The general structure of a CNN alternates convolution layers followed by pooling layers, with the last layers being fully connected (dense). The convolution operation enables performing weighted averaging of inputs such that the network learns filters that are activated when specific spatial patterns in the input are detected. Formally, given input images y and a kernel k , the discrete convolution operator is given by

$$K[s_1, s_2] * y[s_1, s_2] = \sum_{i=-\infty}^{\infty} \sum_{j=-\infty}^{\infty} K[i, j]y[s_1 + i, s_2 + j], \quad (4)$$

where s_1 and s_2 are pixels of the image. The sums are finite in practice since the kernel K has compact support and depends on the number of pixels. Each kernel K is a matrix of trainable weights (also known as filters) applied to small regions of the input image, and the same kernel is translated across the dimensions of the image. Several independently trained

kernels can be applied when multiple filters are used in a convolutional layer. Depending on the values of the kernel weights, one can get different properties associated with the image, such as edges of objects. We refer to Pinaya et al. (2020) for more information on CNNs and to https://tensorflow.org/api_docs for instructions on the TensorFlow implementation of convolutional layers.

3 Proof of concept for max-stable processes

Max-stable distributions are commonly used for studying extreme events recorded in space and time. As a proof of concept, we exemplify the methodology from Section 2 by estimating parameters of max-stable processes. These processes are well known for having full likelihoods that are computationally intractable even in moderate dimensions. However, simulation is manageable. With this example, we aim to demonstrate that our method can accurately recover the parameters of a model with intractable likelihood by learning the mapping from raw data. We use here the algorithm provided by Schlather (2002) for simulation of max-stable models implemented in the `SpatialExtremes` R-package.

In Section 3.1 we briefly outline max-stable distributions and processes and the most commonly used approach for estimating parameters in such models. Sections 3.2 and 3.3 outline the parameter estimation setup and the CNN used in the estimation procedure, respectively. In Sections 3.4 and 3.5 the performance of the CNN estimator is assessed and compared with a benchmark through a simulation study using two popular max-stable models.

3.1 Definition and the pairwise likelihood approach

Consider a sequence of independent and identically distributed (i.i.d.) stochastic processes $Y_1(\mathbf{s}), Y_2(\mathbf{s}), \dots$, where $\mathbf{s} \in \mathcal{S} \subset \mathbb{R}^d$ is a spatial site. A max-stable process Z is the limit process of normalized pointwise block-maximum process (with block size m), provided that sequences of

functions $a_m(\mathbf{s}) > 0$ and $b_m(\mathbf{s})$ exist:

$$Z(\mathbf{s}) = \lim_{m \rightarrow \infty} a_m(\mathbf{s})^{-1} \left[\max_m \{Y_1(\mathbf{s}), \dots, Y_m(\mathbf{s})\} - b_m(\mathbf{s}) \right], \quad \mathbf{s} \in \mathbb{R}^d,$$

in other words, that pointwise maxima of independent copies of $Z(\mathbf{s})$ remain in the same family up to a location and scale functions. Each marginal distribution of $Z(\mathbf{s})$ is a generalized extreme value (GEV) distribution with location, scale, and shape parameters that potentially depend on the spatial locations (De Haan and Ferreira, 2007).

We now introduce a representation that will serve as the basis for constructing a parametric max-stable process in the following sections. Let $\{\xi_i\}_{i \geq 1}$ be the points of a Poisson process on $(0, \infty)$ with intensity $d\Lambda(\xi) = \xi^{-2}d\xi$, and let $W_1(\mathbf{s}), W_2(\mathbf{s}), \dots$ be independent copies of a nonnegative stochastic process such that $W(\mathbf{s}) \geq 0$ with mean equal to one. The processes W_i and the points of the Poisson process $\{\xi_i\}_{i \geq 1}$ are assumed to be independent. Then

$$Z(\mathbf{s}) = \max_{i \geq 1} \xi_i W_i(\mathbf{s}), \quad \mathbf{s} \in \mathcal{S}, \tag{5}$$

is a max-stable process with unit Fréchet margins: $P\{Z(\mathbf{s}) \leq z\} = \exp(-1/z)$, $z > 0$. Suitable choices for $W(\cdot)$ yield to different max-stable processes (Schlather, 2002). In the next sections we will consider two different choices: Brown-Resnick (Kabluchko et al., 2009) and Schlather's model (Schlather, 2002).

- The Brown—Resnick model arises when $W_i(\mathbf{s}) = \exp\{\epsilon_i(\mathbf{s}) - \gamma(\mathbf{s})\}$ in (5), where $\epsilon_i(\mathbf{s})$ are independent copies of a standard stationary Gaussian process such that $\epsilon(\mathbf{0}) = 0$ almost surely and with semivariogram $\gamma(\mathbf{h}) = (\|\mathbf{h}\|/\lambda)^\nu$, where \mathbf{h} is the spatial separation, $\lambda > 0$ is the range, and $\nu \in (0, 2]$ is a smoothness parameter. Brown-Resnick processes are popular in practice because of their flexibility compared with other choices and the ability to generalize several stationary max-stable models, such as the geometric Gaussian model (Davison et al., 2012). For a precise justification of its practical performance, see Thibaud and Opitz (2015).

- The second model is the characterization proposed in Schlather (2002), with $W_i(\mathbf{s}) = \sqrt{2\pi} \max\{0, \epsilon_i(\mathbf{s})\}$, where $\epsilon_1(\mathbf{s}), \epsilon_2(\mathbf{s}), \dots$ are independent copies of a stationary Gaussian process with unit variance and correlation function ρ that is a powered exponential: $\rho(\mathbf{h}) = \exp\{-(\|\mathbf{h}\|/\lambda)^\nu\}$, $\lambda > 0, \nu \in (0, 2]$.

Schlather (2002) showed that one can obtain exact simulations of max-stable models on a finite sampling region if the support of the random Poisson process ξ (see (5)) is either included in a ball $b(o; r)$ or is uniformly bounded by a constant C . For Brown-Resnick and Schlather's models, these conditions are not satisfied since Gaussian processes are not uniformly bounded. However, Schlather (2002) introduced approximations for the constant C such that if $P[\max\{0; \xi_i(\mathbf{s})\} > C]$ is sufficiently small, the simulation procedure is still accurate.

It follows from (5) that the joint cumulative distribution of $Z(\mathbf{s})$ at a finite collection of sites $\{\mathbf{s}_1, \dots, \mathbf{s}_D\} \subset S$ is given by

$$p(Z(\mathbf{s}_1) \leq z_1, \dots, Z(\mathbf{s}_D) \leq z_D) = \exp\{-V(z_1, \dots, z_D)\}, \quad (6)$$

where the exponent function $V(z_1, \dots, z_D) = E[\max\{W(\mathbf{s}_1)/z_1, \dots, W(\mathbf{s}_D)/z_D\}]$, satisfies homogeneity and marginal constraints (De Haan et al., 1984). By differentiating the distribution (6) with respect to its variables z_1, \dots, z_D , one can deduce the corresponding density function, or the full likelihood as

$$f(z_1, \dots, z_D) = \exp\{-V(z_1, \dots, z_D)\} \sum_{\pi \in \mathcal{P}} \prod_{l=1}^L \{-V_{\pi_l}(z_1, \dots, z_D)\}, \quad (7)$$

where \mathcal{P} denotes the collection of all partitions $\pi = \{\pi_1, \dots, \pi_L\}$ of $\{1, \dots, D\}$ and V_{π_l} denotes the partial derivative of the function V with respect to the variables indexed by the set π_l . The sum in Equation (7) is taken over the set of all possible partitions, which equals the *Bell* number of order D . This leads to an explosion of terms even for a moderate D , and the full likelihood quickly becomes intractable. Castruccio et al. (2016) concluded that with modern computer technologies, full likelihood inference is still limited to $D \leq 12$. In the simple bivariate

case, however, the density is computationally tractable, which explains the common practice of adopting the pairwise likelihood in place of the full likelihood (see, e.g., Padoan et al. (2010); Davis et al. (2013); Shang et al. (2015)). The corresponding log weighted pairwise likelihood for model (6) is given by

$$l(\boldsymbol{\phi}) = \sum_{(j_1, j_2) \in \mathcal{P}} \alpha_{j_1, j_2} \left[\log\{V_1(z_{j_1}, z_{j_2})V_2(z_{j_1}, z_{j_2}) - V_{12}(z_{j_1}, z_{j_2})\} - V_1(z_{j_1}, z_{j_2}) \right], \quad (8)$$

where $\boldsymbol{\phi} \in \boldsymbol{\Phi} \subset \mathbb{R}^p$ is the vector of unknown parameters and $\alpha_{j_1, j_2} \geq 0$ denotes the likelihood weight assigned to the pair $\{j_1, j_2\}$. We suppress the dependence of V_1 , V_2 , and V_{12} on $\boldsymbol{\phi}$ for notation simplicity. The weights are often set to one only for pairs of locations up to a certain distance: $\mathbf{h} = \|\mathbf{s}_1 - \mathbf{s}_2\| < \delta$, where $\delta > 0$ is an appropriate cut-off distance chosen, for instance, via cross-validation (Ribatet, 2008). The block maximum recorded at the j th station is denoted by z_j , where $\mathcal{P} = \{(j_1, j_2) : 1 \leq j_1 < j_2 \leq D\}$. For multiple independent replicates of the z_j 's, the maximum pairwise likelihood estimator $\hat{\boldsymbol{\phi}}$ in (8) is strongly consistent and asymptotically Gaussian. The asymptotic variance for such misspecified likelihood estimators is of the sandwich form (Padoan et al., 2010). However, calculating this sandwich variance is time-consuming, since it requires working with four points at a time. The variability of $\hat{\boldsymbol{\phi}}$ may also be assessed by using block bootstrap techniques.

3.2 Proposed parameter estimate setup

For simplicity, we describe below our proposed estimation approach for simulated data on uniform margins, such that we estimate only the dependence parameters. We simulate I independent replicates $(\boldsymbol{\theta}_i, \mathbf{y}_i)_{i=1}^I$ (also known as testing data), where $\boldsymbol{\theta}_i = (\lambda_i^{\text{test}}, \nu_i^{\text{test}})^\top$ are the range and smoothness of the max-stable process and $\mathbf{y}_i = \{y_i(\mathbf{s}_1), \dots, y_i(\mathbf{s}_D)\}^\top$ are the corresponding realizations (either Brown—Resnick or Schalter's). We consider here $I = 16$ parameter scenarios with values of λ_i^{test} and ν_i^{test} on a (not necessarily equally spaced) grid. For each pair $(\lambda_i^{\text{test}}, \nu_i^{\text{test}})$, max-stable samples are generated at $D = 25^2$ (i.e., 25×25 images) in $[0, 20]^2$. We then obtain

estimates of θ_i using two different approaches:

1. CNN estimator $\hat{\theta}_i^{\text{CNN}} = (\hat{\lambda}_i^{\text{CNN}}, \hat{\nu}_i^{\text{CNN}})^\top$: We simulate training data $\mathbf{y}_j^{\text{train}}$ each of size $D = 25^2$ from max-stable models with parameters randomly sampled from $\lambda_j^{\text{train}} \sim \text{Unif}(a_\lambda^{\text{train}}, b_\lambda^{\text{train}})$ and $\nu_j^{\text{train}} \sim \text{Unif}(a_\nu^{\text{train}}, b_\nu^{\text{train}})$, for $j = 1, \dots, 2000$. The choice of a_θ^{train} and b_θ^{train} , for $\theta = \lambda, \nu$, is informed by the testing parameters θ_i to ensure that the training set covers the region of interest. The CNN is trained by using $\log(\mathbf{y}^{\text{train}})$ as the input, where $\mathbf{y}^{\text{train}}$ is a tensor with dimensions $2000 \times 25 \times 25$ and $\left\{ \log(\boldsymbol{\lambda}^{\text{train}}), \log\left(\frac{\boldsymbol{\nu}^{\text{train}}}{2 - \boldsymbol{\nu}^{\text{train}}}\right) \right\}^\top$ as the output with size 2000×2 . The logarithm is used here as a variance-stabilizing transformation to help with numerical issues during training, and the denominator corresponding to ν is chosen so that this parameter is not greater than two. Once trained, the CNN is used to return predictions $\hat{\theta}_i^{\text{CNN}}$ based on logarithm-transformed testing images \mathbf{y}_i , for $i = 1, \dots, 16$.
2. Pairwise-likelihood estimator $\hat{\theta}_i^{\text{PL}} = (\hat{\lambda}_i^{\text{PL}}, \hat{\nu}_i^{\text{PL}})^\top$: The models are fitted to data by using the pairwise likelihood (see (8)) through the R-function `fitmaxstab`. This function performs optimization using another R-function, `optim`, and we set the method to L-BFGS-B. After a small cross-validation study, we find that including pairs that are more than three units apart worsens the estimation, besides increasing the fitting time. Therefore, we combine only likelihood contributions from pairs that are at most three units apart with equal weights $\alpha_{i_1, i_2} = 1$, and the remaining weights are set to zero. We initialize the parameters by giving the optimizer multiple random starting pairs around the actual values. Then we run the full optimization from the five pairs with the highest pairwise likelihood among the random pairs as the starting point. We show the results using the pair with the pairwise likelihood maximizer as initial values.

Layer Type	Output Shape	Filters	Kernel Size	Parameters
2D conv	$[-, 25, 25, 128]$	128	3×3	1280
2D conv	$[-, 13, 13, 128]$	128	3×3	147584
2D conv	$[-, 7, 7, 16]$	16	3×3	18448
dense	$[-, 4]$			1028
dense	$[-, 8]$			40
dense	$[-, 16]$			144
dense	$[-, 2]$			34
Total trainable weights:				168,558

Table 1: Summary of the CNN model. It is a sequential model taking input of shape $[-, 25, 25, 128]$ and mapping it to two scalar values of shape $[-, 2]$.

3.3 CNN architecture

We use a sequential CNN taking simulated images as input and mapping it onto two scalar values. Table 1 provides a summary of the settings used to train the CNN using simulated data from the Brown-Resnick and Schlather’s model. We report the number of layers and how they transform the dimension of the input tensors. For example, the first row of Table 1 shows that the model input is a tensor of shape $[-, 25, 25, 128]$, where ‘-’ indicates an arbitrary number of samples, the number ‘25’ relates to the dimension of the images, and ‘128’ stands for the number of filters. Then, the first convolution layer transforms the input tensor into another tensor of output shape $[-, 13, 13, 128]$ by using 128 filters with a kernel size of 3×3 (see the second row).

The proposed CNN consists of three pairs of convolutions with varying numbers of filters. We keep three dense layers at the end of the network with 8, 16, and 2 units. The total number of trainable weights of the CNN is 168,558. For all the layers, we use the rectified linear unit (ReLU) activation function, which has been shown to be beneficial for regression type models (Hastie et al., 2009). The implementation of our algorithms is carried out by using TensorFlow/Keras built in the R-software. The CNN weights are initialized randomly; and to train the network, we employ the widely used Adam optimizer (Kingma and Ba, 2014) with a learning rate of 0.01. The training is performed for 32 epochs, where in each epoch the CNN weights are updated utilizing a batch size of 40 samples from the full training dataset, which here consists of $J = 2000$ samples.

3.4 Results for the Brown-Resnick model

In this section we show a comparison between CNN and pairwise likelihood for estimating the parameters of a Brown-Resnick model. A description of this model is given in Section 3.1, and details of the parameter estimation set up for both methods can be found in Section 3.2. The testing set comprises 16 pairs of simulated parameters and data, where the parameters are all possible combinations $(\lambda^{\text{test}}, \nu^{\text{test}})^\top$, with $\lambda^{\text{test}} \in [0.50, 0.75, 1.00, 1.50]$ and $\nu^{\text{test}} \in [0.80, 1.05, 1.30, 1.55]$. For each combination, which we call a scenario, we simulate 50 i.i.d. realizations of the respective Brown-Resnick process, which will be used to assess the uncertainty of the estimators. Examples of realizations covering the simulated parameters are illustrated in Figure 1 (a).

The training set for the CNN has output values drawn from $\lambda_j^{\text{train}} \sim \text{Unif}(0.1, 3)$ and $\nu_j^{\text{train}} \sim \text{Unif}(0.5, 1.9)$, $j = 1, \dots, 2000$, so that it covers the range of the true output by a reasonable margin. Once the network has converged, we use it to predict Brown-Resnick parameters on the test data. Scatterplots of the estimated transformed range ($\log(\lambda)$) versus transformed smoothness ($\log\{\nu/(2-\nu)\}$) (with the number on the axes in the original scale) from the CNN (green) and pairwise likelihood (red) are displayed in Figure 2 (a). The \times symbol in each plot represent the truth. Each scatterplot comprises 50 independent data replicates that are estimated independently. When fitting the pairwise likelihood, we notice the importance of using the maximizer among multiple starting values (we used 20 values around the true and performed full optimization from the five pairs with the highest pairwise likelihood; see Section 3.2 for details). This figure shows that the CNN works consistently well, whereas the pairwise likelihood performance varies between scenarios. As expected from estimating long-range dependencies, there is an increased variability for larger values of this parameter, especially from the pairwise likelihood estimator. In particular, the pairwise likelihood tends to underestimate the smoothness parameter. This is more evident when the range and smoothness are both large (see bottom right corner of Figure 2 (a)). For large smoothness, there were a few data replicates for which the pairwise likelihood failed to estimate both parameters (see the last row of Figure 2 (a)). For

rougher fields with medium ranges, there is a large variability in the estimates, in most cases underestimating the smoothness. Based on this study, the CNN results in an overall more minor estimation bias and variance than the pairwise likelihood, with most estimations closer to the actual parameter values.

Table 2 reports values of root mean squared error (RMSE), mean absolute error (MAE), and mean bias from predicting Brown-Resnick parameters $(\lambda; \nu)$ using the CNN and pairwise likelihood approaches. Each score is the result of 50 replicates and the 16 scenarios combined. Results for the Brown-Resnick model (columns 2 and 3) confirm that the CNN estimator outperforms the pairwise likelihood overall. This is more evident for the smoothness parameter, with higher biases and RMSEs and MAEs about 1.6 and 2.7 times larger for the pairwise likelihood. Biases resulting from pairwise likelihood estimates are in accordance with the scatterplots in Figure 2 (a) and might be explained by the low efficiency of using only pairs of variables. Moreover, we consider one replicate for each test data, and increasing this number could make the estimation more stable for the pairwise. However, investigating higher-order composite likelihood methods is outside this paper’s scope, and we refer the reader to Genton et al. (2011) for details on this approach.

3.5 Results for Schlather’s model

Similarly to the experiment for the Brown-Resnick model described in the preceding section, we simulate testing sets from Schlather’s model comprising 50 independent copies of 16 parameter scenarios of size $D = 25^2$ in $[0, 20]$. Here, the parameters $(\lambda^{\text{test}}, \nu^{\text{test}})^\top$ used to simulate data consist of all pair combinations from $\lambda^{\text{test}} \in [0.50, 1.50, 2.0, 2.5]$ and $\nu^{\text{test}} \in [0.80, 1.05, 1.30, 1.55]$. The dataset to train the CNN contains simulated images of the same size where the range and smoothness are generated according to $\lambda_j^{\text{train}} \sim \text{Unif}(0.1, 3)$ and $\nu_j^{\text{train}} \sim \text{Unif}(0.5, 1.8)$, $j = 1, \dots, 2000$. Figure 1 (b) shows examples of simulations from the Schlather’s model. This model produces data that are more noisy and presents a more challenging scenario when compared with

the Brown-Resnick process presented in the preceding section (see Figure 1 (a)).

Each scatterplot in Figure 2 (b) displays estimated values of $\log(\lambda)$ versus $\log\{\nu/(2-\nu)\}$ for 50 replicates and a different scenario where the estimation is performed by using either the CNN (green) or pairwise likelihood (red). Compared with the analyses for Brown-Resnick processes (see Figure 2 (a)), both methods produce estimates with less variability, and the bias from the pairwise is less prominent here. Exceptions are scenarios with small ranges for which the pairwise likelihood underestimates the range in a few datasets (see the first column of Figure 2 (b)). The CNN produces small biases when predicting both parameters and all scenarios, and the variability is slightly larger for large-range cases. The results suggest that the CNN estimator performs well overall and constantly improves the pairwise likelihood results. We notice that the accuracy of the CNN is regardless of the range of training values since all the estimates under CNN are never near the boundary of the range of simulated parameter values. Although only small biases arise from the pairwise likelihood in estimating the range for most parameter values, in a couple of instances the method performed poorly, producing estimates about two to three times smaller than the true ones. In contrast, the CNN estimates larger ranges well, and outliers are extremely unlikely to occur.

The improved pattern from the CNN over the pairwise likelihood estimator is confirmed in Table 2, with RMSE and MAE values that are around 60% to 80% smaller. The only case where the pairwise likelihood beats the CNN is in terms of mean biases for the smoothness parameter, which is primarily seen for small ranges, namely, when the spatial dependence is relatively weak (see Figure 2 (b)). In such cases the CNN estimates of smoothness seem to have a distribution that is not strongly dependent on the actual smoothness. The computations were carried out on the 8-core processor Intel Core i9 with 2.4 GHz. The elapsed times (in seconds) for fitting and predicting the parameters, excluding the time for producing training samples, from the Brown-Resnick and Schlather's models from the CNN are 58 and 45, respectively. In contrast, for the pairwise likelihood, these times are 1,305 and 14,960, respectively. The CNN-based parameter

estimation, excluding the time for producing training samples, reduced the computational time by a fraction of 300. Overall, similarly to what we observed for the Brown-Resnick model, the CNN provides better results than does the pairwise likelihood, requiring massively less computational resources. The success of the CNN confirms our previous conclusions. It even more strongly supports the need for alternative methods to overcome the difficulty of the suboptimal approaches currently used to fit intractable models. Moreover, such results are expected to improve in higher-dimensional settings, where the loss in efficiency of pairwise likelihood estimators is more significant.

	Brown-Resnick		Schlather's	
	CNN	PL	CNN	PL
RMSE	0.45;0.38	0.56;0.62	0.66;0.49	0.83;0.62
MAE	0.14;0.11	0.24;0.30	0.33;0.18	0.55;0.31
Mean Bias	0.09;-0.02	0.05;-0.15	-0.23;0.01	0.12;-0.02

Table 2: RMSE, MAE, and mean bias from the Brown-Resnick and Schlather's models using the CNN and the pairwise likelihood approaches. The two numbers in each column for the first three rows represent scores for estimating range and smoothness, respectively.

4 Application to temperature data

In this section we discuss an application of our method to a surface temperature reanalysis dataset, which we describe in Section 4.1. Section 4.2 outlines the estimation framework and highlights the additional steps needed to estimate parameters from real data compared with the simulation study in Section 3. In Section 4.3 we analyze the results.

4.1 NLDAS data and preprocessing

Reanalysis temperature data are extracted from the North American Land Data Assimilation System (NLDAS-2) (Mitchell et al., 2004; Xia et al., 2012b,a) and are freely available at <https://ldas.gsfc.nasa.gov/nldas/v2/models>. NLDAS data is quality-controlled and available at a grid spacing of 12 km and the hourly temporal resolution. Hourly data are extracted between 1991 and 2019.

We select locations in the midwestern United States on a 107×55 grid-scale and perform spatial downsampling by selecting 25 equally spaced points in the latitude and longitude directions so that images are the same size as in the simulation study (see Section 3). To decrease the effect of seasonality, we restrict the data to 60 days over April-May, although there is still large variability within this period. We consider daily minima, and the models are fit to the negative of this quantity over six 10-day blocks, resulting in 174 datasets of size 25×25 . Figure 3 shows images of minimum temperature data from the six 10-day data blocks over April-May (rows 1-6) at four equally spaced years between the 29 years available (rows 1-4). As expected, temperature minimas are lower at the beginning of April.

Although the spectral representation of max-stable processes in (5) relies on Fréchet margins, in practice the observations are rarely a unit Fréchet distribution. We follow the usual approach of fitting a GEV distribution before transforming the data to the unit Fréchet scale. We model marginal distributions with GEVs using componentwise minima over six 10-day blocks at each site separately. We estimate a single scale and shape parameter for the considered April-May period. In contrast, the location parameter is specific to each of the six 10-day blocks to better meet the identically distributed assumption. Quantile-quantile plots (not shown) suggest that a GEV reasonably approximates marginal distributions. Images of the estimated locations, scale, and shape are displayed in Figure 5. Location parameters for each of the 10-day blocks gradually increase as the weather gets warmer. Shape parameters are primarily negative, indicating a bounded upper tail. Negative shape parameter estimates are commonly found when fitting GEV distributions of temperature extremes; see, for example, Kharin and Zwiers (2000); Huang et al. (2016). Exceptions are close to the Great Lakes (see mid-upper right corner), where the positive shape parameter implies a heavy tail. We then use these estimated parameters from the GEV to transform the data to the unit Fréchet scale.

4.2 Implementation details of the estimation framework

In Section 3 we generated the training set for the CNN based on the data and parameters from the testing set, which were simulated and were therefore known. In this section the parameters of the testing set are unknown. Consequently, we first need to define a range of parameter values that reflect the assumed max-stable distribution of the unit Fréchet transformed data. The diagram in Figure 4 illustrates the several steps needed to obtain parameter estimates of max-stable processes using the temperature data. Notice that in the simulated setup described in Section 3, only steps 4, 5, 6, and 7 were needed. Different approaches can be taken to choose the region to sample the parameters from. We present one possible method, where the permissible parameter region from fitting a pairwise likelihood to the data is expanded by simulating data in a broader grid with uniform probabilities.

The first task is to fit Brown-Resnick models to each of the 174 transformed data images separately by using the pairwise likelihood estimator (8), for which pairs of locations are at most three units apart. Figure 6 displays histograms of the pairwise likelihood (red) estimated range (left) and smoothness (right). Whereas the range parameter varies from approximately 12% to 50% of the total size of the domain $[0, 20]$, the estimated smoothness is often relatively large. Next, we train the CNN with simulated training data of size 2,000 generated by sampling both parameters independently from uniform distributions. The lower and upper bounds of the uniform are obtained by perturbing the pairwise likelihood estimates based on their standard deviations:

$$\begin{aligned}\lambda_j^{\text{train}} &\sim \text{Unif}\{\hat{\lambda}_{\min}^{\text{PL}} - 3 \times \text{sd}(\hat{\boldsymbol{\lambda}}^{\text{PL}}) \wedge 0, \hat{\lambda}_{\max}^{\text{PL}} + 3 \times \text{sd}(\hat{\boldsymbol{\lambda}}^{\text{PL}})\}, \quad j = 1, \dots, 2000 \\ \nu_j^{\text{train}} &\sim \text{Unif}\{\hat{\nu}_{\min}^{\text{PL}} - 3 \times \text{sd}(\hat{\boldsymbol{\nu}}^{\text{PL}}) \wedge 0, \hat{\nu}_{\max}^{\text{PL}} + 3 \times \text{sd}(\hat{\boldsymbol{\nu}}^{\text{PL}}) \wedge 2\}, \quad j = 1, \dots, 2000,\end{aligned}\quad (9)$$

where $a \wedge b$ denotes the maximum between a and b , $\hat{\boldsymbol{\Theta}}^{\text{PL}} = (\hat{\Theta}_1^{\text{PL}}, \dots, \hat{\Theta}_{174}^{\text{PL}})^\top$, $\hat{\Theta}_{\min}^{\text{PL}} = \min(\hat{\Theta}_1^{\text{PL}}, \dots, \hat{\Theta}_{174}^{\text{PL}})$ and $\hat{\Theta}_{\max}^{\text{PL}} = \max(\hat{\Theta}_1^{\text{PL}}, \dots, \hat{\Theta}_{174}^{\text{PL}})$ for $\Theta = \lambda, \nu$. Using the range and smoothness values generated from (9), we simulate Brown-Resnick processes with spatial dimension

$D = 25^2$. We then train a CNN model using the logarithm transformed data from these simulations as inputs and the variance stabilizing transformation on the outputs (see Section 3.3 for details). The CNN model configuration is summarized in Table 3. After the model is trained, we predict the output based on input images of logarithm transformed data. Histograms of estimated parameters at their original scale from the CNN are displayed in Figure 6 (green). Compared with the pairwise likelihood estimates (red), the range parameter (left) estimated from the CNN is usually larger and more uniform across datasets. The smoothness (right) is closer to normally distributed with a higher probability of values close to one.

Layer Type	Output Shape	Filters	Kernel Size	Parameters
2D conv	$[-, 25, 25, 128]$	128	3×3	1280
2D conv	$[-, 13, 13, 128]$	128	3×3	147584
2D conv	$[-, 7, 7, 128]$	16	3×3	147584
2D conv	$[-, 4, 4, 16]$	16	3×3	18448
dense	$[-, 4]$			260
dense	$[-, 8]$			72
dense	$[-, 8]$			72
dense	$[-, 2]$			18
Total trainable parameters:				315,358

Table 3: Summary of the CNN model. It is a sequential CNN taking inputs of shape $[-, 25, 25, 1]$ and mapping it to two scalar values of shape $[-, 2]$.

4.3 Results

We detail here the results from the CNN and pairwise likelihood approaches with the data and implementation described in the preceding sections. For clarity, the results are presented on the Fréchet transformed data scale.

A useful quantity to visualize spatial extremes is the so-called extremal coefficient $\theta(\mathbf{s}_1; \mathbf{s}_2) \in [1, 2]$, $\mathcal{D} = \{\mathbf{s}_1; \mathbf{s}_2\}$, giving a measure of extremal dependence between two stationary max-stable random fields, $Z(\mathbf{s}_1)$ and $Z(\mathbf{s}_2)$, where $\theta(\mathbf{s}_1; \mathbf{s}_2) = 1$ corresponds to perfect dependence and $\theta(\mathbf{s}_1; \mathbf{s}_2) = 2$ to independence. The modified version of a variogram, called F-madogram, proposed by Cooley et al. (2006), is defined as $v_F(\mathbf{s}_1; \mathbf{s}_2) = 0.5 \times \mathbb{E}\{|F[Z(\mathbf{s}_1)] - F[Z(\mathbf{s}_2)]|\}$, where $F(z) =$

$\exp(-1/z)$ are unit Fréchet margins. The F-madogram is used here as a summary statistic for the extremal coefficient through the relation $2v_F(\mathbf{s}_1; \mathbf{s}_2) = \frac{\theta(\mathbf{s}_1; \mathbf{s}_2) - 1}{\theta(\mathbf{s}_1; \mathbf{s}_2) + 1}$.

The left panel of Figure 7 compares the empirical F-madogram estimates (black dots) of the extremal coefficients between pairs of sites, plotted against the spatial distance $\mathbf{h} = \|\mathbf{s}_i - \mathbf{s}_j\|$, with respect to their pairwise likelihood (red curve) and CNN (green curve) model counterparts. The empirical F-madogram is calculated from 174 datasets at the 25^2 locations, and estimates of the binned F-madogram for the two models are obtained by using 100 bins. The pairwise likelihood fit appears to underestimate extremal dependence at distances greater than five (red curve is generally above the black dots). In contrast, the CNN provides a more realistic estimation of spatial dependence, matching empirical and estimated extremal coefficients.

The uncertainty from both model fits can be assessed from the right panels of Figure 7, which show nonbinned estimated F-madograms of the extremal coefficients based on 200 simulations from Brown-Resnick processes using as parameter values the estimates obtained from one of the images in the testing set. For this example, the CNN (green) estimates a considerable larger range parameter compared with the pairwise likelihood (red) ($\hat{\lambda}_i^{\text{CNN}} = 28.6$ and $\hat{\lambda}_i^{\text{PL}} = 8.9$), which better matches the empirical spatial dependence (see black dots in the left panel). Consequently, only the CNN can capture pairs with high extremal dependencies (e.g., $\theta(\mathbf{h}) < 1.5$), a feature that is more evident at larger spatial separation (the green area is below the red in the rightmost plot).

The quantile-quantile plots in Figure 8 compare the observed and predicted minima (left), mean (middle), and maxima (right) from the pairwise likelihood (red) and CNN (green) estimates using 200 simulated replicates for each test data and all the 25^2 sites. Overall 95% confidence intervals calculated by using quantiles from the simulations are also shown with solid lines. The CNN outperforms the pairwise likelihood for the lower quantiles and for predicting minima and mean. For maxima and moderate quantiles, the estimated values are below the diagonal for pairwise likelihood and above for CNN, suggesting that the spatial dependence in the extremes

is underestimated by the pairwise likelihood and overestimated by the CNN. More significant maxima quantiles are overestimated by both methods, although the uncertainty is higher since there are fewer cases in the dataset.

5 Discussion

In this work we have proposed a new approach to estimate parameters in statistical models based on deep neural networks. As a proof of concept, we have tested the methodology based on the highly challenging problem of inference for max-stable distributions and processes. We illustrated the benefit of using deep NN models over the classical pairwise likelihood approach through simulated and real-world data. Results from our simulation study for the popular Brown–Resnick and Schlather’s models showed better performances (more negligible bias and variance) of our method compared with the current approach with speedups in computations. Unlike pairwise likelihood, the proposed deep learning approach relies on simulations of the full model and does not involve approximations of spatial dependence.

We follow the paradigm that if it is possible to simulate from a model, one can perform inference. Our approach uses data from simulations as input to a deep NN and learns to predict statistical parameters. Similar to the well-known ABC, the idea is that the deep NN becomes a stand-in for compressing data and recognizing model parameters. However, a key difference from ABC is that our method automatically maps data and parameters inside the deep NN, eliminating the problem of choosing summary statistics and metrics to compare data. Another difference is that in ABC the entire estimation procedure must be run again from scratch for each individual dataset, whereas in the proposed framework the estimation is performed upfront in a single training phase, followed by a cheaper prediction phase able to handle multiple testing sets. Moreover, our new approach benefits from recent advances in algorithms for conventional deep NNs, which can learn features automatically from highly complex images while being fast and easy to apply. Problems with our approach will emerge when there are many parameters in

the model, up to a point where generating training data for high-dimensional parameter spaces becomes practically intractable.

In this work we have focused on modeling multivariate extremes and followed a proof of concept approach. We can use the same idea presented here for inferring parameters in other statistical models. In particular, non-Gaussian models for dependencies tend to be hard to estimate by using classical approaches. Extensions for future work include nonhomogeneous Poisson processes (Moller and Waagepetersen, 2003), epidemiology models (Lawson, 2008), discrete stochastic population dynamics models (Wood, 2010), and random set models.

In summary, we show that deep NN models are easy to construct, are fast to fit, and show promising results for performing statistical inference, especially when the usual techniques fail.

References

- Castruccio, S., Huser, R., and Genton, M. G. (2016). High-order composite likelihood inference for max-stable distributions and processes. *Journal of Computational and Graphical Statistics*, 25(4):1212–1229.
- Cooley, D., Naveau, P., and Poncet, P. (2006). Variograms for spatial max-stable random fields. In *Dependence in Probability and Statistics*, pages 373–390. Springer.
- Creel, M. (2017). Neural nets for indirect inference. *Econometrics and Statistics*, 2:36–49.
- Cremanns, K. and Roos, D. (2017). Deep Gaussian covariance network. *arXiv preprint arXiv:1710.06202*.
- Davis, R. A., Klüppelberg, C., and Steinkohl, C. (2013). Statistical inference for max-stable processes in space and time. *Journal of the Royal Statistical Society: SERIES B: Statistical Methodology*, pages 791–819.
- Davison, A. C., Padoan, S. A., Ribatet, M., et al. (2012). Statistical modeling of spatial extremes. *Statistical Science*, 27(2):161–186.
- De Haan, L. et al. (1984). A spectral representation for max-stable processes. *The Annals of Probability*, 12(4):1194–1204.
- De Haan, L. and Ferreira, A. (2007). *Extreme Value Theory: An Introduction*. Springer Science & Business Media.

- Erhardt, R. J. and Smith, R. L. (2012). Approximate Bayesian computing for spatial extremes. *Computational Statistics & Data Analysis*, 56(6):1468–1481.
- Friedman, J., Hastie, T., Tibshirani, R., et al. (2001). *The Elements of Statistical Learning*, volume 1. Springer Series in Statistics.
- Genton, M. G., Ma, Y., and Sang, H. (2011). On the likelihood function of Gaussian max-stable processes. *Biometrika*, pages 481–488.
- Gerber, F. and Nychka, D. W. (2020). Fast covariance parameter estimation of spatial Gaussian process models using neural networks. *Stat*, page e382.
- Hastie, T., Tibshirani, R., and Friedman, J. (2009). *The Elements of Statistical Learning: Data Mining, Inference, and Prediction*. Springer Science & Business Media.
- Huang, W. K., Stein, M. L., McInerney, D. J., Sun, S., and Moyer, E. J. (2016). Estimating changes in temperature extremes from millennial-scale climate simulations using generalized extreme value (gev) distributions. *Advances in Statistical Climatology, Meteorology and Oceanography*, 2(1):79–103.
- Huser, R., Davison, A. C., and Genton, M. G. (2016). Likelihood estimators for multivariate extremes. *Extremes*, 19(1):79–103.
- Huser, R., Dombry, C., Ribatet, M., and Genton, M. G. (2019). Full likelihood inference for max-stable data. *Stat*, 8(1):e218.
- Jiang, B., Wu, T.-y., Zheng, C., and Wong, W. H. (2017). Learning summary statistic for approximate Bayesian computation via deep neural network. *Statistica Sinica*, pages 1595–1618.
- Juba, B. and Le, H. S. (2019). Precision-recall versus accuracy and the role of large data sets. In *Proceedings of the AAAI Conference on Artificial Intelligence*, volume 33, pages 4039–4048.
- Kabluchko, Z., Schlather, M., De Haan, L., et al. (2009). Stationary max-stable fields associated to negative definite functions. *The Annals of Probability*, 37(5):2042–2065.
- Kharin, V. V. and Zwiers, F. W. (2000). Changes in the extremes in an ensemble of transient climate simulations with a coupled atmosphere–ocean gcm. *Journal of Climate*, 13(21):3760–3788.
- Kingma, D. P. and Ba, J. (2014). Adam: A method for stochastic optimization. *arXiv preprint arXiv:1412.6980*.

- Lawson, A. B. (2008). *Bayesian disease mapping: hierarchical modeling in spatial epidemiology*. Chapman and Hall/CRC.
- Liu, K., Ok, K., Vega-Brown, W., and Roy, N. (2018). Deep inference for covariance estimation: Learning Gaussian noise models for state estimation. In *2018 IEEE International Conference on Robotics and Automation (ICRA)*, pages 1436–1443. IEEE.
- Mitchell, K. E., Lohmann, D., Houser, P. R., Wood, E. F., Schaake, J. C., Robock, A., Cosgrove, B. A., Sheffield, J., Duan, Q., Luo, L., et al. (2004). The multi-institution north american land data assimilation system (NLDAS): Utilizing multiple GCIP products and partners in a continental distributed hydrological modeling system. *Journal of Geophysical Research: Atmospheres*, 109(D7).
- Moller, J. and Waagepetersen, R. P. (2003). *Statistical inference and simulation for spatial point processes*. CRC Press.
- Padoan, S. A., Ribatet, M., and Sisson, S. A. (2010). Likelihood-based inference for max-stable processes. *Journal of the American Statistical Association*, 105(489):263–277.
- Paszke, A., Gross, S., Chintala, S., Chanan, G., Yang, E., DeVito, Z., Lin, Z., Desmaison, A., Antiga, L., and Lerer, A. (2017). Automatic differentiation in pytorch.
- Pinaya, W. H. L., Vieira, S., Garcia-Dias, R., and Mechelli, A. (2020). Convolutional neural networks. In *Machine Learning*, pages 173–191. Elsevier.
- Radev, S. T., Mertens, U. K., Voss, A., Ardizzone, L., and Köthe, U. (2020). Bayesflow: Learning complex stochastic models with invertible neural networks. *IEEE Transactions on Neural Networks and Learning Systems*.
- Ribatet, M. (2008). SpatialExtremes: An R-package for modelling spatial extremes. *R Package Version*, pages 2–0.
- Ribatet, M., Cooley, D., and Davison, A. C. (2012). Bayesian inference from composite likelihoods, with an application to spatial extremes. *Statistica Sinica*, pages 813–845.
- Rudi, J., Bessac, J., and Lenzi, A. (2021). Parameter estimation with dense and convolutional neural networks applied to the Fitzhugh-Nagumo ODE. *Mathematical and Scientific Machine Learning*.
- Schlather, M. (2002). Models for stationary max-stable random fields. *Extremes*, 5(1):33–44.

- Shang, H., Yan, J., and Zhang, X. (2015). A two-step approach to model precipitation extremes in California based on max-stable and marginal point processes. *The Annals of Applied Statistics*, pages 452–473.
- Stephenson, A. and Tawn, J. (2005). Exploiting occurrence times in likelihood inference for componentwise maxima. *Biometrika*, 92(1):213–227.
- Tawn, J. A. (1988). Bivariate extreme value theory: models and estimation. *Biometrika*, 75(3):397–415.
- Thibaud, E., Aalto, J., Cooley, D. S., Davison, A. C., Heikkinen, J., et al. (2016). Bayesian inference for the Brown–Resnick process, with an application to extreme low temperatures. *The Annals of Applied Statistics*, 10(4):2303–2324.
- Thibaud, E. and Opitz, T. (2015). Efficient inference and simulation for elliptical Pareto processes. *Biometrika*, 102(4):855–870.
- Varin, C., Reid, N., and Firth, D. (2011). An overview of composite likelihood methods. *Statistica Sinica*, pages 5–42.
- Wood, S. N. (2010). Statistical inference for noisy nonlinear ecological dynamic systems. *Nature*, 466(7310):1102–1104.
- Xia, Y., Mitchell, K., Ek, M., Cosgrove, B., Sheffield, J., Luo, L., Alonge, C., Wei, H., Meng, J., Livneh, B., et al. (2012a). Continental-scale water and energy flux analysis and validation for north american land data assimilation system project phase 2 (NLDAS-2): 2. validation of model-simulated streamflow. *Journal of Geophysical Research: Atmospheres*, 117(D3).
- Xia, Y., Mitchell, K., Ek, M., Sheffield, J., Cosgrove, B., Wood, E., Luo, L., Alonge, C., Wei, H., Meng, J., et al. (2012b). Continental-scale water and energy flux analysis and validation for the north american land data assimilation system project phase 2 (NLDAS-2): 1. intercomparison and application of model products. *Journal of Geophysical Research: Atmospheres*, 117(D3).
- Xu, X. and Reid, N. (2011). On the robustness of maximum composite likelihood estimate. *Journal of Statistical Planning and Inference*, 141(9):3047–3054.

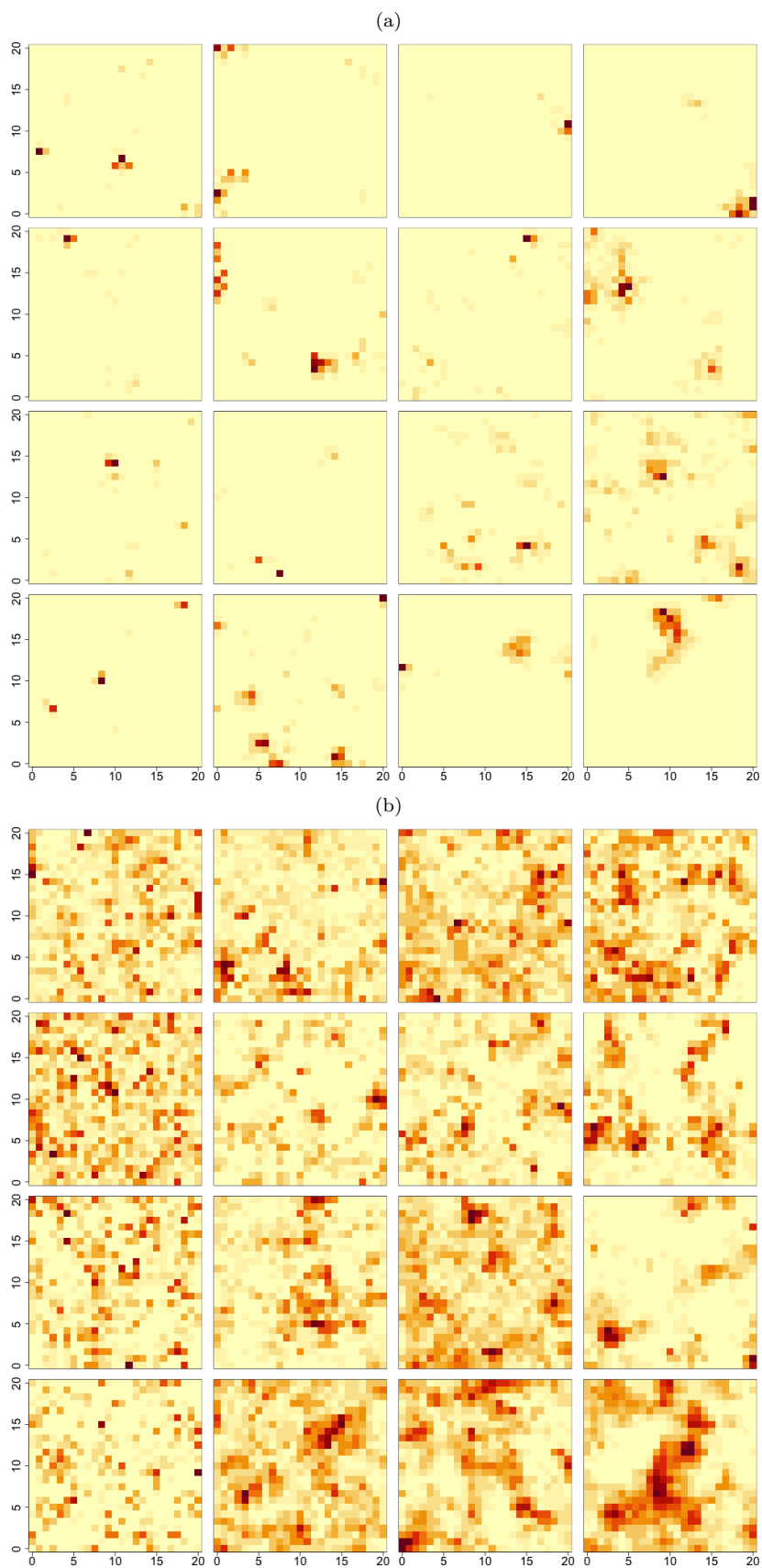


Figure 1: Simulations from the Brown–Resnick (a) and Schlather’s (b) models on 25×25 images covering $[0, 20]^2$. Small to large range values (λ) are shown from left to right and rough to smooth (ν) processes are from top to bottom.

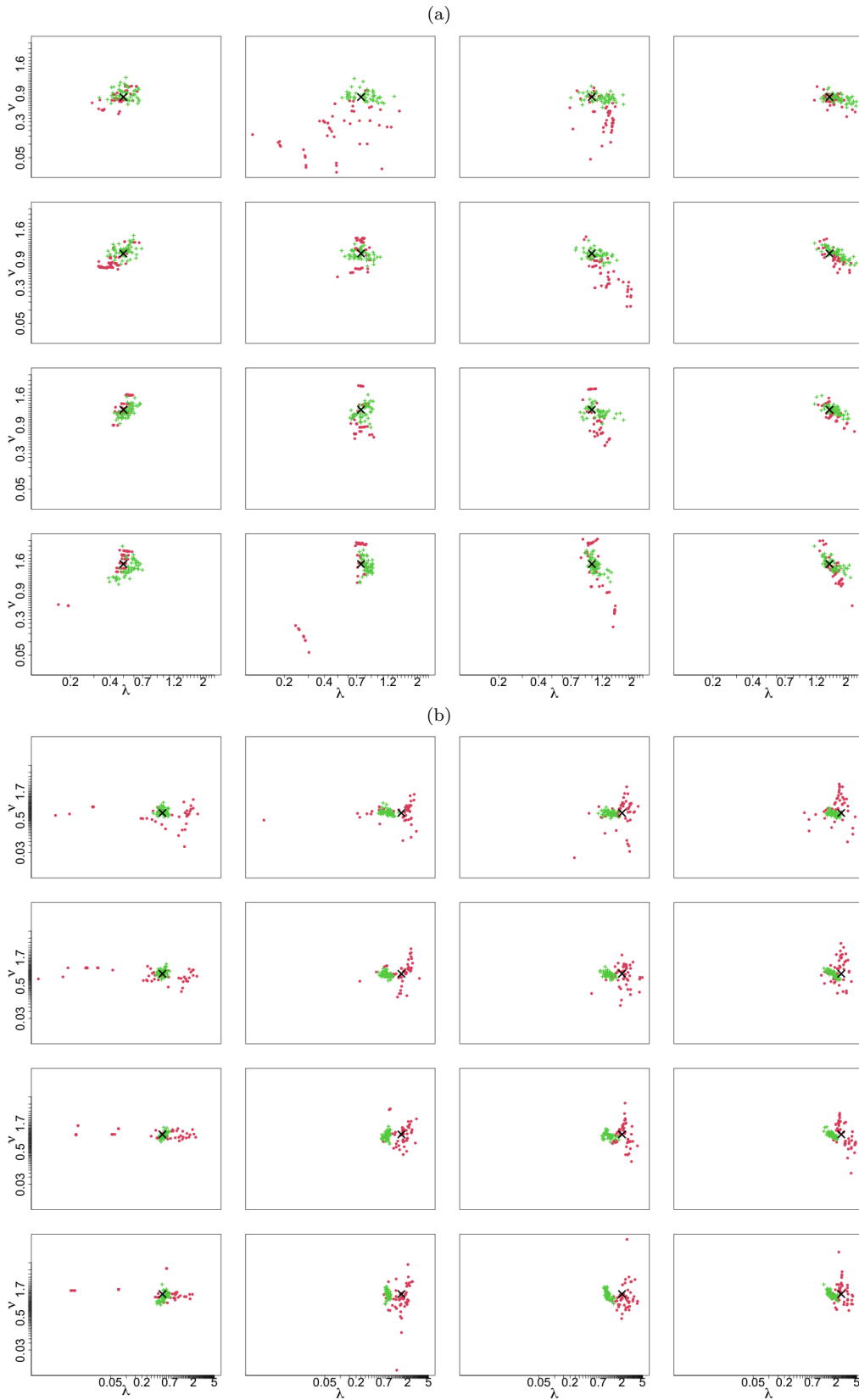


Figure 2: Scatterplots of estimated parameters on the transformed scales (with numbers on the axes on the untransformed scales). Each plot shows 50 independent estimates from the Brown-Resnick (a) and Schlather's (b) models using the CNN (green) or PL (red) with the first initial values that maximizes the PL (red). Small to large ranges are shown from left to right, and rough to smooth are from top to bottom. The \times 's are the true values.

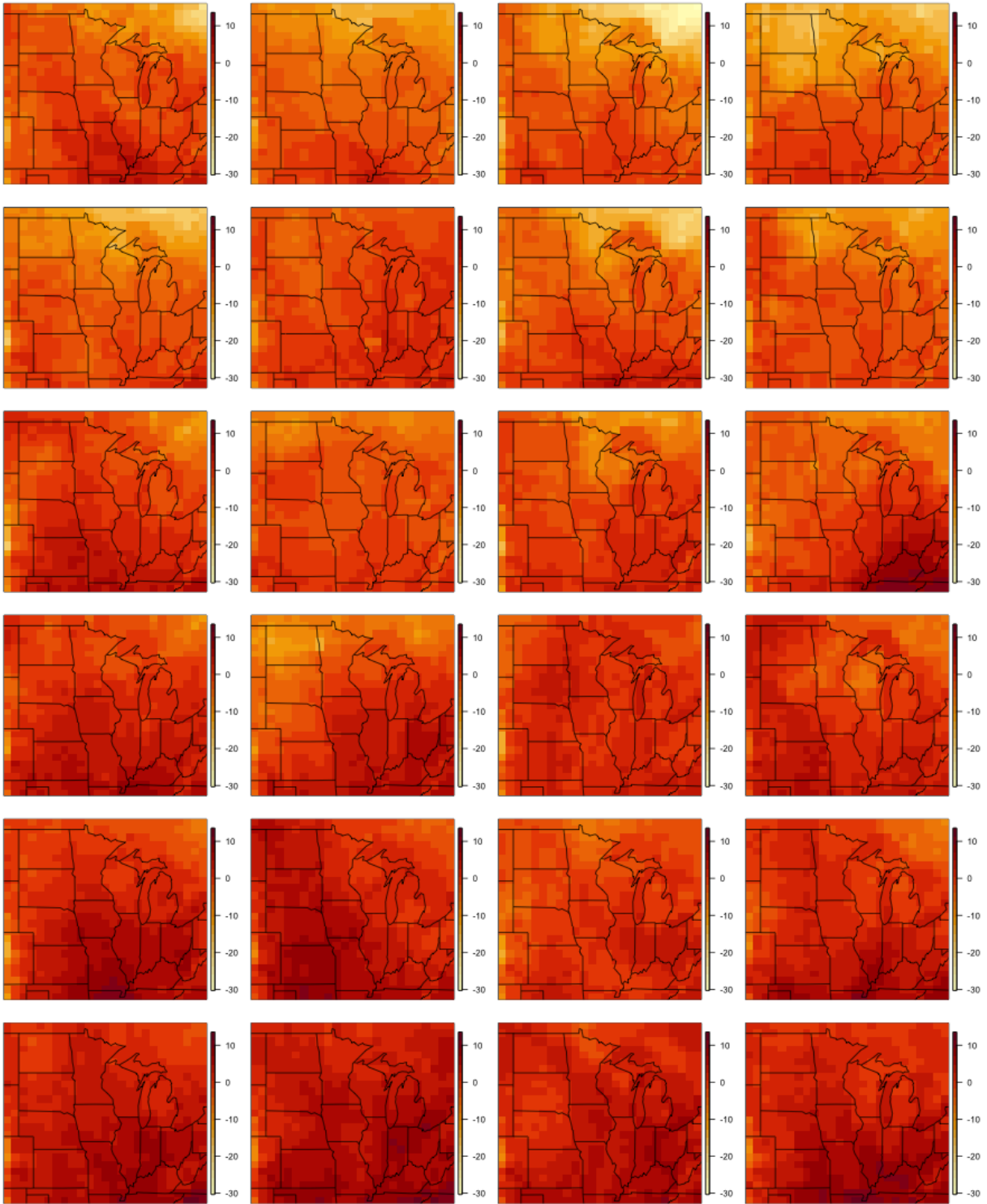


Figure 3: Temporal evolution of temperature minima from six 10-day data blocks over April-May (rows 1-6) during 1991, 2000, 2009, 2019 (columns 1-4).

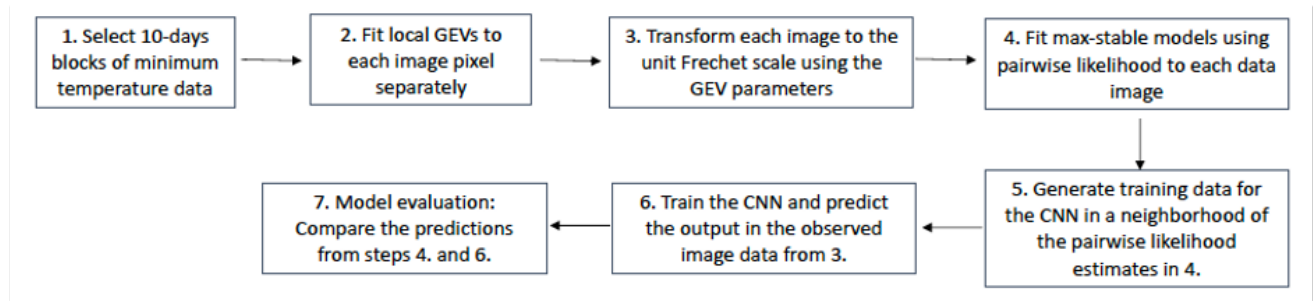


Figure 4: Diagram of the proposed framework for estimating parameters from temperature data. Knowledge about the mapping between simulated data and parameters is compactly encoded within the weights of the CNN.

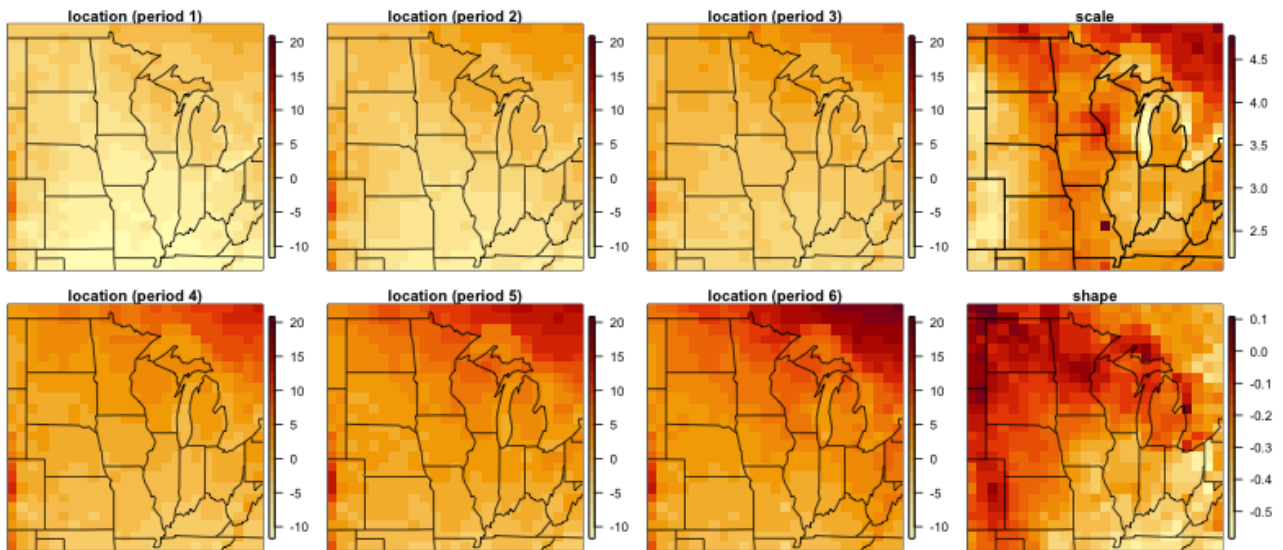


Figure 5: (a) Estimated location for each of the 6 blocks of data, scale, and shape parameters obtained from the individual fit of the GEV model.

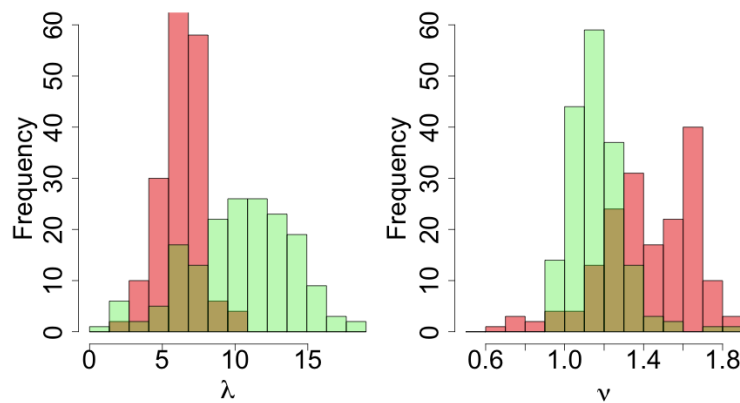


Figure 6: Histograms of the estimates of range (left) and smoothness (right) from a Brown-Resnick model fitted to the Fréchet transformed data by using pairwise likelihood (red) and CNN (green).

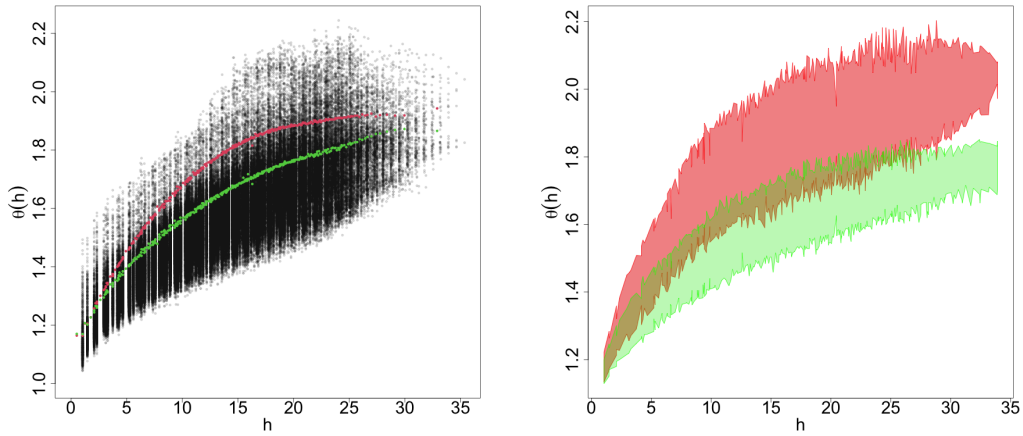


Figure 7: Left: F-madogram estimates for the validation datasets (black points) and the estimated extremal coefficient functions from the pairwise likelihood (red) and CNN (green) using 100 bins. Right: Example of nonbinned F-madogram estimates using as parameter values the estimates obtained from one of the images in the testing set.

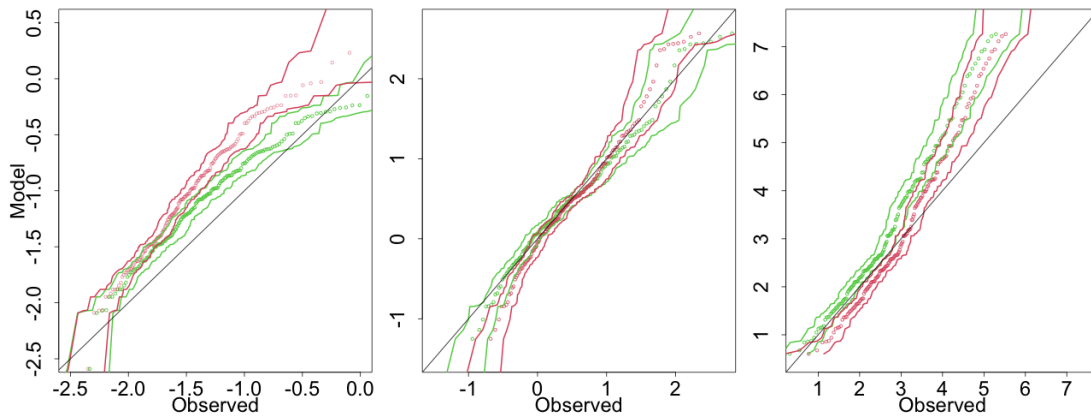


Figure 8: Comparison of the observed versus predicted minima (left), mean (middle), and maxima (right) with 95% confidence intervals from the pairwise likelihood (red) and CNN (green) fits.